JOURNAL OF SPACECRAFT AND ROCKETS
Vol. 29, No. 3, May-June 1992

Supersonic Flow over an Axisymmetric Backward-Facing Step

E. Loth*
University of Illinois at Urbana-Champaign, Urbana, Illinois 61801
K. Kailasanath†
Naval Research Laboratory, Washington, D.C. 20375
and
R. Löhner‡
George Washington University, Washington, D.C. 20052

Large eddy numerical simulations of supersonic flows over an axisymmetric backward-facing step have been completed using a recently developed axisymmetric version of the finite element method-flux corrected transport algorithm, FEM-FCT. The code is based on the mixing layer and recompression premises of the Chapman-Korst model. It solves the time-accurate Euler equations utilizing 1) adaptive unstructured gridding to resolve flow feature details and 2) a conservative nonlinear scheme to capture features in the compressible flowfield. This approach may be employed since the location of the separation point is fixed at the sharp corner. The simulation allows the large-scale structures present in the mixing layer to interact dynamically with the recompression region. Comparisons have been made with available experimental data for a range of Mach numbers and step height to step radius ratios for which boundary-layer effects are not pronounced. In general, good agreement between predictions and measurements was found for 1) the time-averaged surface pressure distributions along the backstep and the reattachment wall, 2) the flowfield structure in general, and 3) the downstream reattachment lengths. Effects of axisymmetry were noted in flowfield characteristics such as increased base pressure, curvature of expansion fans, stronger recompression shocks, and higher Mach number levels in the subsonic recirculating region.

Nomenclature

e = specific total energy of flow
F = fluxes of conserved quantity
h = step height (defined as positive if toward the axis of symmetry)
M = Mach number
p = pressure
R = radius upstream of step about axis of symmetry
r = radial coordinate
S = source term to conservation equations
t = time
U = conserved quantity
u = velocity component parallel to axis of symmetry
v = radial velocity component
x = coordinate along axis of symmetry
δ = upstream boundary-layer thickness
γ = specific heat ratio
ρ = density

Subscripts
b = conditions along step, base conditions
h = high-order scheme
l = low-order scheme
r = reattachment point
∞ = condition upstream of step

Superscripts
i = coordinate summation
n = timestep level

Presented as Paper 90-1580 at the AIAA 21st Fluid Dynamics, Plasmadynamics, and Lasers Conference, Seattle, WA, June 18-20, 1990; received May 23, 1991; revision received Dec. 3, 1991; accepted for publication Jan. 2, 1992. This paper is declared a work of the U.S. Government and is not subject to copyright protection in the United States.

*Assistant Professor, Department of Aeronautical and Astronautical Engineering. Member AIAA.
†Head, Center for Reactive Flow and Dynamical Systems, Laboratory for Computational Physics and Fluid Dynamics. Associate Fellow AIAA.
‡Research Professor, Civil, Mining, and Environmental Engineering, School of Engineering and Applied Science. Member AIAA.

Introduction

SEVERAL applications including ballistics, spacecraft in planetary atmosphere, such as the Space Shuttle,[1] and applications in supersonic mixing may directly benefit from further understanding the flow behind an axisymmetric rearward-facing step in supersonic flow. In addition, experimental investigations of flow recirculation and reattachment at supersonic speeds are commonly studied in the backward-facing step configuration.[2-12]

Such a flowfield can be generically described as a supersonic freestream of Mach number M_∞ that turns in the direction of the rearward-facing step through an expansion fan, with a resulting mixing layer between the supersonic fluid above and the subsonic recirculating region below (Fig. 1). The pressure in the recirculating region is generally uniform, is below that of the freestream pressure p_∞, and is termed the base pressure. As the mixing layer impinges on the downstream wall, the flow turns back toward the freestream direction and a recompression shock wave is formed. In such a flowfield, the upstream boundary layer is defined as thin if it has a thickness δ that is smaller than either the radius of symmetry R or the step height h.

The pressure at the base portion of such flowfields has long been predicted with the Chapman-Korst type models.[2,13-18] Such models assume a stagnant flow for the recirculating region and link the inviscid gas dynamics with the turbulent mixing layer typically with an assumed constant pressure mixing theory for velocity and energy profile. To close the set of unknowns, a recompression criteria is imposed that usually assumes that a discriminating streamline stagnates through an essentially isentropic process. This discriminating streamline indicates the slowest flow tube that contains sufficient energy to match the recompression pressure rise given by the oblique

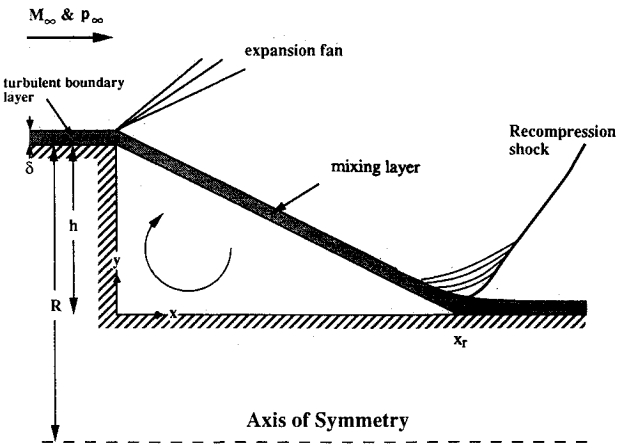

Fig. 1 Sketch of supersonic flow over an axisymmetric rearward-facing step.

shock at the end of the separated flow region. Such asymptotic models were intended to treat flows with very high Reynolds numbers, i.e., flows in which the mixing layer is both turbulent and fully developed. Empirical functions are often used to bring the recompression model into better agreement with the experiment.[2,18] Such improvements are typically based on variations of the recompression process, such as different heights above the wall at which it occurs or the width of the turbulent shear layer spreading.

Shapiro[19] notes that measurements for two-dimensional and axisymmetric supersonic backsteps indicate two types of flows: 1) flowfields where the boundary layer upstream of the step is either laminar or of comparable thickness as the step height, and 2) flowfields where the upstream boundary layer is fully developed, turbulent, and small compared with the step height. The first type typically produces base pressures and flow structures that vary considerably as a function of Reynolds number and boundary-layer characteristics, whereas for an M_∞ of at least 2 the second type typically shows little deviation of base pressure and flow structure, i.e., such flows are essentially Reynolds number independent.[12]

To allow more generality and complex geometry for predicting such flows, full field computational fluid dynamic solutions have been recently employed; these were primarily structured mesh finite difference schemes[20-22] that included a variety of empirical turbulence models. These calculations exhibited reasonable flow features and base pressures that were typically within 20–30% of experimental results. It should be noted that several researchers have recently shown that supersonic turbulent mixing layers behave much differently than their subsonic counterparts, and this may have a direct impact on the turbulence model predictions.[23] Recently, there has been increased focus on unstructured adaptive grids because of their ability to provide fine grid resolution near shocks and other compressible flow features.

Therefore, the premise of this study was to employ a time accurate scheme using adaptive unstructured grids and a robust shock capturing scheme. For this flow, separation is readily specified to occur at the corner of the backward-facing step, with a subsequent mixing layer that was free to develop large-scale structures that result from the natural shear instability. The adaptive mesh refinement can provide high resolution of the mesh in areas of significant density gradients to resolve the critical flow features such as mixing layer dynamics and shock recompression, whereas the shock-capturing scheme provides crisp and monotonic descriptions of shock structures and contact discontinuities while allowing second-order accuracy elsewhere.

Much of the mixing layer dynamics may be captured since this solution is time accurate and can resolve (due to the adaptive refinement) the large-scale structures that have been shown to characterize the main features of the flow.[24] The large eddy simulation is based on the premise that the large-scale structures dominate the turbulent diffusion aspects as compared with the inherent artificial viscosity of the numerical method. Such a methodology holds promise to predict axisymmetric base pressure flows with similar agreement as those of the Chapman-Korst models without having to specify stagnant flow conditions in the recirculating region or model the recompression dynamics. However, agreement with experiment might only be expected for Reynolds number independent flows, i.e., thin turbulent boundary layers approaching the step and an M_∞ of at least 2.

Employment of the recently developed axisymmetric finite element method-flux corrected transport (FEM-FCT) scheme[25] allowed an evaluation of the model's predictive capabilities as well as further insight into the characteristics associated with supersonic flow over an axisymmetric backstep. The objective of the time-dependent calculations was to represent the basic time-averaged features of the flow without resorting either to a full compressible direct Navier-Stokes solution that is computationally expensive or to an empirically based turbulence model solution.

There are a few nonintrusive experimental studies of supersonic flow over an axisymmetric backstep with an upstream boundary layer that is thin and fully developed. Fortunately, such axisymmetric flows are not subject to the end wall effects of plane flows that can significantly alter the flow characteristics.[5] The Roshko and Thomke study[5] included a large ducted axisymmetric body in a supersonic wind tunnel with a downstream facing step along its circumference. The ratio of step height to upstream body radius h/R was varied from 0.28 to 0.042, and M_∞ was varied from 2.09 to 4.37. Surface static pressure measurements were made along the wall providing base pressure and subsequent surface pressure recovery. Surface oil flow visualization was used to determine flow reattachment points along with spark shadowgraphs to provide shock and mixing layer locations.

Other available studies were generally limited to base pressure measurements and schlieren photographs. These include Chapman[12] with an h/R range of 0.4–1.0 and an M_∞ range of 2.0–2.9, Bogdonoff[3] with an h/R of 0.75 and an M_∞ of 2.95, and Donaldson[4,8] with an h/R range of 0.78–1.0 and an M_∞ of 1.99. In addition, Nash[26] has measured two-dimensional ($h/R = 0.0$) base pressures for a range of M_∞ from 1.5 to 5.0. From the previous studies, data were selected on the basis of evidence of a thin, fully developed, turbulent boundary layer before to the backstep (the criteria for a thin boundary layer for this study was a δ less than both $h/2$ and $R/2$) and an M_∞ of at least 2. In both prediction and experiment, the back pressure is low enough to provide supersonic flow downstream of the step.

In addition to the previous axisymmetric (Fig. 2a) and two-dimensional (Fig. 2b) backstep flows, the sudden expansion axisymmetric backstep flow (Fig. 2c) has also been studied by Zelenkov[27] as well as Blagosklonov and Khomutov.[28] These studies documented experimental base pressures (pressure along the step wall), and Zelenkov[27] presented an analytical description of base pressure similar to Chapman-Korst models that provided reasonable correlation with experimental data.

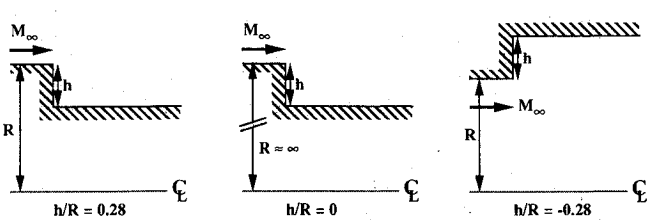

Fig. 2 Sketch of various axisymmetric backward-facing step geometries.

Numerical Method

The gas dynamic equations for axisymmetric compressible flow can be written as follows:

$$\begin{bmatrix} r\rho \\ r\rho u \\ r\rho v \\ r\rho e \end{bmatrix}_t + \begin{bmatrix} r\rho u \\ r\rho u^2 + rp \\ r\rho uv \\ ru(\rho e + p) \end{bmatrix}_x + \begin{bmatrix} r\rho v \\ r\rho uv \\ r\rho v^2 + rp \\ rv(\rho e + p) \end{bmatrix}_r = \begin{bmatrix} 0 \\ 0 \\ p \\ 0 \end{bmatrix} \tag{1}$$

where x and r denote the axial and radial coordinates; ρ, p, and e denote the density, pressure, and specific total energy; u and v denote the velocities in the x and r directions; and the lower subscripts refer to taking the derivative quantity of the expression. Written in this form, Eq. (1) can be discretized to form a conservative scheme, which is important to be able to predict sharp discontinuities such as shocks. We then assume an ideal gas equation of state of the form

$$p = (\gamma - 1)\rho[e - \tfrac{1}{2}(u^2 + v^2)] \tag{2}$$

The two-step Taylor-Galerkin algorithm has been used extensively for the computation of inviscid and viscous flows for the Cartesian coordinate system[29-33] and recently for a few axisymmetric examples by Löhner et al.,[25] where the code development is discussed. The scheme is basically an explicit two-step discretization of the system of partial differential equations given in Eq. (1):

$$\frac{dU}{dt} + \frac{dF^i}{dx^i} = S \tag{3}$$

where U, F^i, and S denote the vector of unknowns, fluxes, and source terms and where tensor notation is used. The two steps of this second-order scheme are then

$$U^{n+\frac{1}{2}} = U^n + \frac{\Delta t}{2}\left(S|^n - \frac{dF^i}{dx^i}\Big|^n\right) \tag{4}$$

$$\Delta U^n = U^{n+1} - U^n = \Delta t\left(S|^{n+\frac{1}{2}} - \frac{dF^i}{dx^i}\Big|^{n+\frac{1}{2}}\right) \tag{5}$$

where n is the timestep level.

Spatial discretization is performed via the Galerkin weighted residual method; however, we note that for step 1 the quantities U, F, and S are assumed piecewise constant in each element, and for step 2 they are assumed piecewise linear. For discretization, interpolation was formed on the quantities (ρ, ρu, ρv, ρe, and r), which leads to a higher accuracy in the r direction[34] and at the same time avoids the singularity problem at $r = 0$, since the scheme is cell centered and the element radius is simply taken as the average of the radii on its corners. In addition, the weighted residual statements necessary for the finite element scheme can be derived in closed form with such a formulation.

In addition to the high-order scheme given above by Eqs. (4) and (6), U_h (which can be made essentially fourth order in phase accuracy), two types of artificial viscosity are added to the scheme. The first is mass diffusion, which is added to yield a monotonic low-order scheme U_l at time $n + 1$. This is combined with the high-order scheme through the FEM-FCT[29] formulation as follows:

$$U^{n+1} = U_l + \text{limit}(\Delta U_h - \Delta U_l) \tag{6}$$

where ΔU_h and ΔU_l denote the increments obtained by the high- and low-order scheme advanced one timestep from U^n, and the "limit" is carried out such that no overshoot or undershoot occurs in the solution.[29] To maintain strict conservation, this limiting is carried out on the element level.[25] This nonlinear contribution through flux corrected transport has been shown to be highly robust and accurate for several fluid dynamics problems using both finite difference schemes (see Oran and Boris[35]) and finite element schemes.[29,31,33,36] In addition, the modified Lapidus artificial viscosity,[30] which proved successful for Cartesian coordinate systems, is extended to the axisymmetric case by simply multiplying the contributions by the average element radius.

Adaptive remeshing was employed to optimize the distribution of grid points for a flowfield not known a priori. Such regridding may reduce storage and CPU requirements by 10–100 times in advection dominated flows as compared with an overall fine grid.[32,37] The remeshing was accomplished using an advancing front generation scheme where local grid size was determined by the level of gradients (both first and second derivative) through a normalized error indicator.[38] Remeshing criteria include allowable stretching levels and the number of smoothing passes for the new grid. Typically, four remeshes with a specified maximum element stretching of two were sufficient for the present flowfields based on previous experience.[25,29,32]

Boundary conditions for the axisymmetric backstep problem are as follows: 1) no flux and no normal velocity along the surfaces, 2) uniform (no boundary layer) inflow conditions beginning one-half step width upstream of the step corner, and 3) free outflow conditions for the top and rear of the computational domain. The separation region was found to be sensitive to the boundary conditions applied in the near region of the step corner. At the corner point, the velocity vector was set to be free. To enforce the parallel wall condition, the predicted velocity component normal to the wall was set equal to zero with the tangential velocity component set upward along the base wall. Rotating the velocity vector along the wall as suggested by Mavriplis[39] (as opposed to projecting the vector as was done here) did not produce any significant change in the results. Proper care was taken such that the flux contributions derived from the corner velocities were consistent with zero flux condition along the back face of the step.

Since there were intrinsic mixing layer fluctuations due to the large eddy formation and dynamics, time-averaging of the fully developed computations was employed for comparison with time-averaged experimental data. Doubling the number of grid points for the simulation of $M_\infty = 2.09$ and $h/R = 0.28$ did not produce significant variation in the time-averaged results (less than 5%) and thus it was felt that the initial resolution, which is shown in the results (Figs. 4–9), would be sufficient for the remainder of the cases studied. No explicit subgrid or viscous modeling was incorporated other than the high frequency filter that the FCT scheme naturally provides (which effectively damps out all spatial frequency below the local cell size). All computations were performed on a Cray X-MP 2/4, and each case took typically less than an hour of Cray CPU time to provide time-averaged distributions.

Results and Discussion

Typical Flowfield

Flowfields and their resulting wall pressure distributions were found for various step height ratios (-0.8, -0.32, 0.0, 0.042, 0.17, 0.28, 0.50, 0.75) and freestream Mach numbers (2.09, 3.02, 3.9). An example of a flowfield downstream of a step is shown in the shadowgraph[40] (Fig. 3) from the experimental investigation of Roshko and Thomke[5] for a freestream Mach number of 2.09 and a step height ratio of 0.28. From the corner going downward, one may observe the shear layer on the photograph indicating the flow separation at the corner. Downstream of this point a dark recompression region can be observed that indicates the high speed fluid is being turned parallel to the wall as reattachment occurs. The recompression shock front appears to become sharp at a vertical position of roughly $h/3$ above the lower wall surface. Note that, as the mixing layer impinges on the wall near the shock foot, its interaction with the boundary results in enhancement of the thickness of the boundary layer that subsequently grows rapidly.

Figure 4 shows an instantaneous solution depicting roughly 60 contours of density throughout the computational domain for the aforementioned Mach 2.09 case. At the shoulder, the expansion fan is evident by the decrease in density. Also, from the corner, the mixing layer is clearly resolved along its entire length. One may note the close comparison with the photograph in Fig. 3 for the inclination angle of the mixing layer to the reattachment wall. An oblique shock of the same angle as in the experiment is also observed along with a thick mixing layer continuing along the wall.

Figure 5 shows the finite element computational mesh that has adapted to the computational flow solution by optimally refining regions of high flow gradients resulting with roughly 7300 nodes (that is typical of the resolution used for the other cases). The areas that include the initial expansion region, the mixing layer, and the oblique shock are all resolved with significantly smaller elements whereas the regions in which relatively weak or smooth flow changes are occurring are resolved only to the preset maximum element size allowed by the remeshing.

Figure 6 shows the pressure contours for the previous case. The expansion fan is readily seen, and, as expected, there is relatively no pressure jump across the mixing layer. Thus, the high-speed flow turns through an expansion fan emanating from the corner, resulting in a higher Mach number and a lower pressure, which is essentially equal to that of the recirculating zone, i.e., the base pressure. As the finite thickness mixing layer approaches the lower wall surface, it tends to bend along the wall giving rise to compression waves above. These waves coalesce over a finite region to form an oblique shock wave a small distance above the mixing layer. In fact, this gradual turning of the mixing layer as it impinges on the wall results in a nonabrupt compression along the wall observed experimentally and numerically. In general, the recompression shock was found to increase in strength for higher levels of M_∞ and as h/r was increased from $-\infty$ to 1.

The downward turning of the expansion fan away from the corner is an axisymmetric effect, not observed in the two-dimensional case. It is due to the decrease in cross-sectional area as the flow turns toward the axis; flow turning through the expansion fan far from the corner experiences a greater reduction in radius and thus must turn additionally to achieve the same overall pressure decrease along the fan. This results in a shorter downstream distance for interaction of the expansion fan with the oblique shock wave, and this interaction results in a weakened recompression shock. As expected, this effect was found to be more pronounced as the absolute value of the step height to body radius ratio $|h/R|$ was increased and was less pronounced as M_∞ was increased.

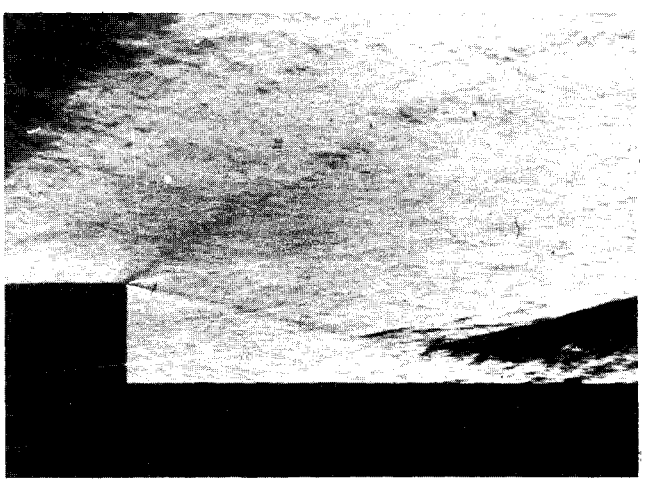

Fig. 3 Shadowgraph photograph[34] for $M_\infty = 2.09$ and $h/R = 0.28$.

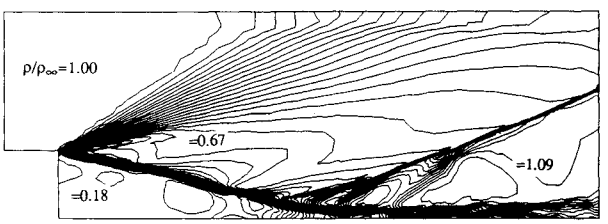

Fig. 4 Predicted density contours for $M_\infty = 2.09$ and $h/R = 0.28$.

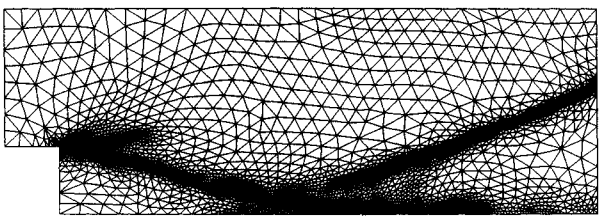

Fig. 5 Finite element mesh for $M_\infty = 2.09$ and $h/R = 0.28$.

Fig. 6 Predicted pressure contours for $M_\infty = 2.09$ and $h/R = 0.28$.

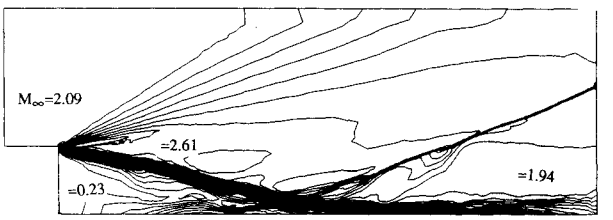

Fig. 7 Predicted Mach number contours for $M_\infty = 2.09$ and $h/R = 0.28$.

Figure 7 shows the Mach number contours for the same case, where a strong change in flow speed from roughly Mach 2.61 to Mach 0.23 occurs across the mixing layer, which continues along the downstream wall and contains nearly all of the vorticity for this flowfield. The subsonic Mach numbers of the recirculating zone tend to increase as the step height ratio h/R is increased from $-\infty$ to 1, and more dramatically as M_∞ is increased from 2.09 to 3.9. The velocity vectors are shown in Fig. 8 and provide further visualization of the expansion fan, the subsonic recirculating zone, the mixing layer, and the oblique shock.

Base Pressure Distributions

The time-averaged lower wall surface pressure distributions are shown in Figs. 9–11 for $h/R = 0.28$ and M_∞ of 2.09, 3.02, and 3.9, respectively. One can see that both experiment[5] and simulation are in reasonable agreement with a relatively constant low pressure near the shoulder followed by a small dip (preceded by a small rise for the $M_\infty = 2.09$ case) and then a pressure rise that initiates at roughly two to three step heights downstream, and ending with a relatively level high pressure region. Note that the recompression region has forced the downstream pressure to be higher than the upstream pressure p_∞ due to effects of axisymmetry, i.e., a reduction in radius. As M_∞ increases, the base pressure ratio p_b/p_∞ drops substan-

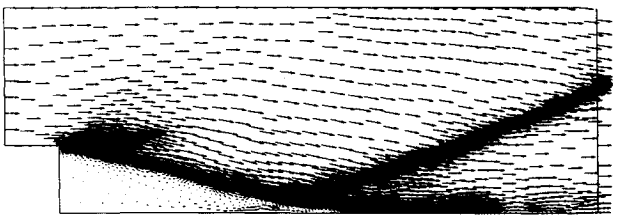

Fig. 8 Predicted velocity vectors for $M_\infty = 2.09$ and $h/R = 0.28$.

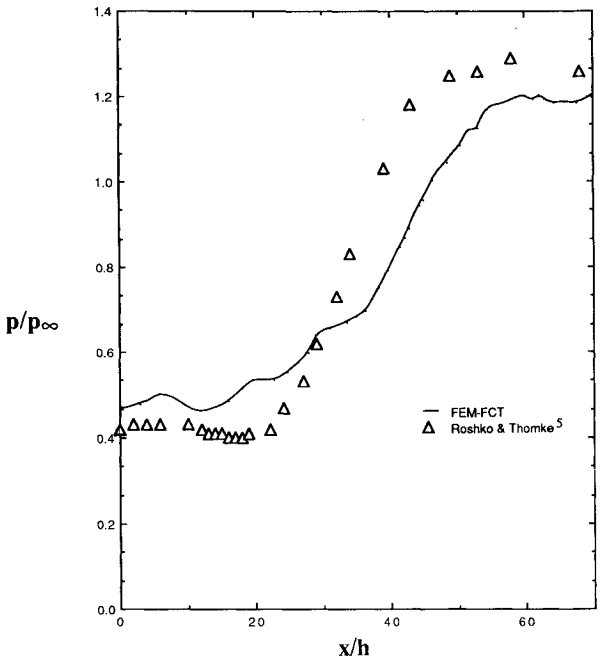

Fig. 9 Lower wall surface pressure distribution for $M_\infty = 2.09$ and $h/R = 0.28$.

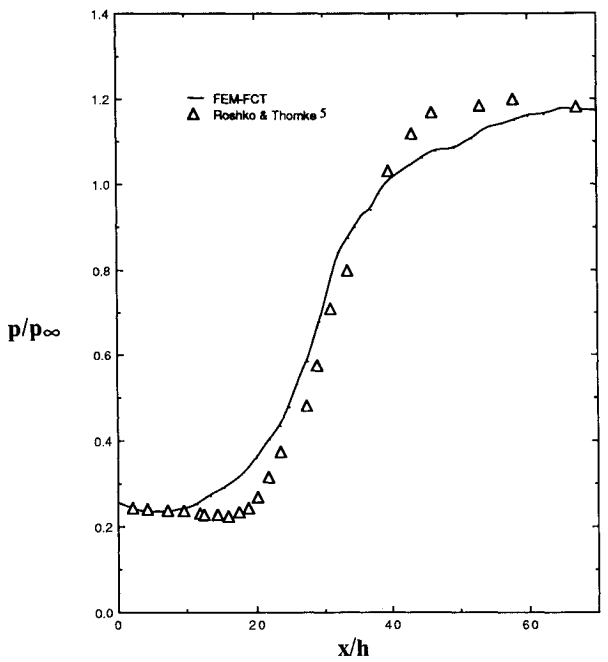

Fig. 10 Lower wall surface pressure distribution for $M_\infty = 3.02$ and $h/R = 0.28$.

tially. This trend is attributed to the larger turning the flow can support at higher Mach numbers and still maintain an oblique recompression shock, which experiments have confirmed. This results in reduced reattachment downstream distance as M_∞ increases. The hump in the pressure rise for the $M_\infty = 3.9$ case may be due to the presence of a lip shock, which is a viscous separation effect[9] that would not be present in the simulations.

Figure 12 shows the corresponding wall pressure distribution for an M_∞ of 2.09 and a relatively small h/R of 0.042. This flow exhibits a more two-dimensional (as opposed to axisymmetric) behavior as noted by the smaller increase of final downstream pressure compared with upstream pressure. The reasonable agreement observed for this distribution is somewhat surprising since the experimental δ/h approached ½ for this case, as opposed to the above cases where δ/h values were about 1/10. However, the measurements[5] also observed remarkable independence of the pressure distribution after recompression had been initiated, even for δ/h values above one.

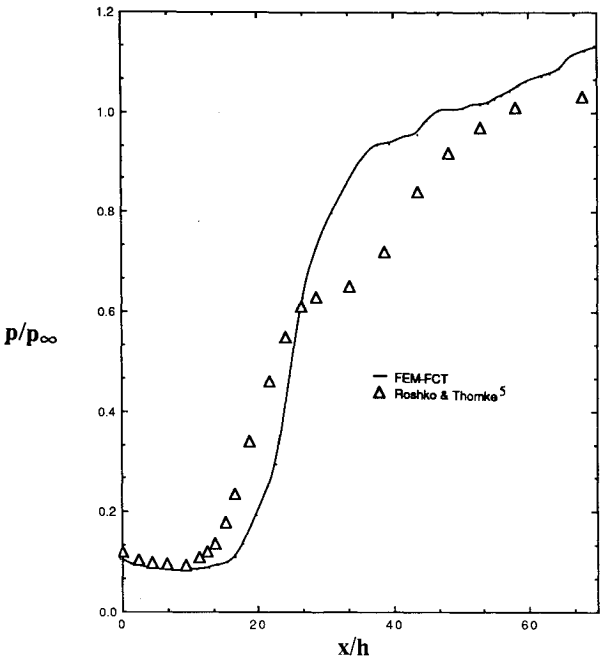

Fig. 11 Lower wall surface pressure distribution for $M_\infty = 3.90$ and $h/R = 0.28$.

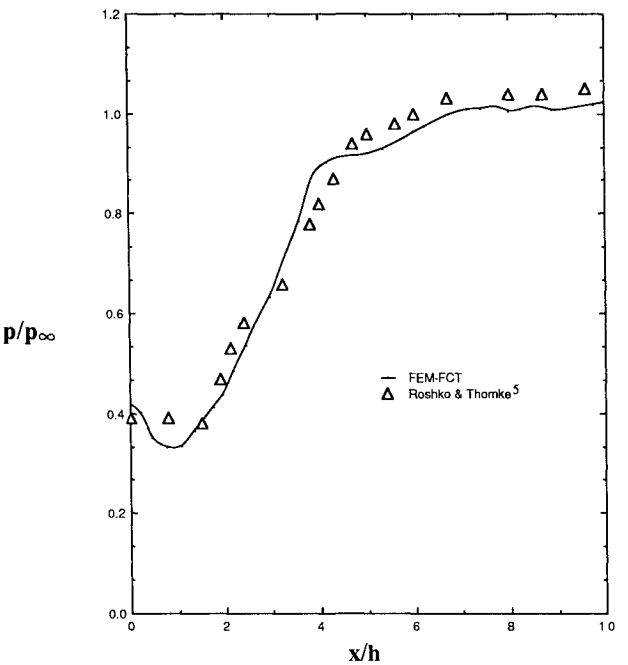

Fig. 12 Lower wall surface pressure distribution for $M_\infty = 2.09$ and $h/R = 0.042$.

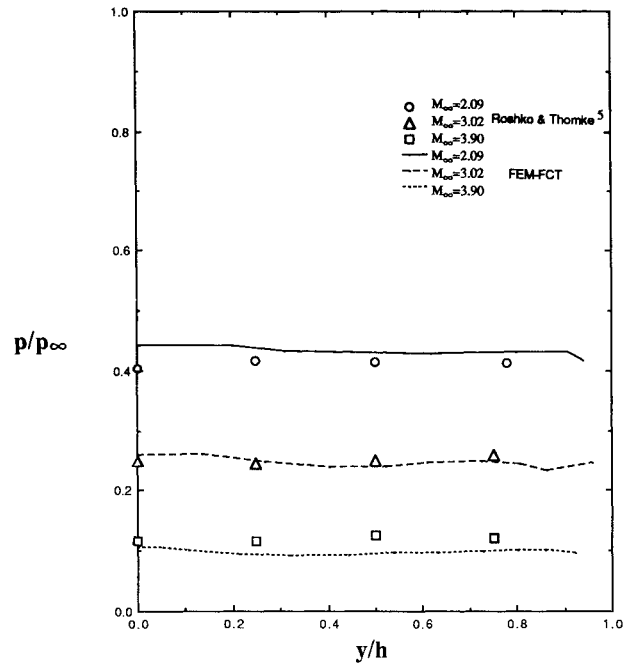

Fig. 13 Vertical step surface pressure distribution for $h/R = 0.28$.

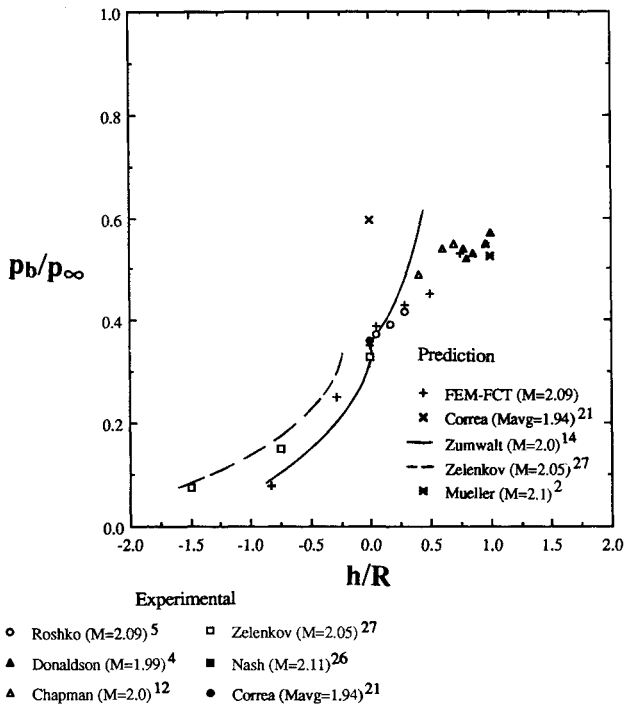

Fig. 14 Base pressure as a function of step height ratio (h/R) for $M_\infty = 2.09$.

Further evidence of the code's ability to predict base pressure distribution is shown in Fig. 13, where static pressure along the rear face of the step is shown for both measurement and simulation. Both the predictions and experimental data show a relatively uniform pressure distribution, which is typical of other axisymmetric base pressure distributions,[15] and indicates that the subsonic region below the mixing layer is one of nearly uniform pressure. The reduction in the base pressure as the Mach number is increased from 2.09 to 3.9 is clearly illustrated, and the agreement between experiment and prediction of base pressure is reasonable.

To determine effects of varying step height ratios, experimental and computational base pressure ratios were plotted as a function of h/R for $M_\infty = 2.09$ and 3.02 in Figs. 14 and 15 (results for similar Mach numbers are also presented). From these figures one may observe the increase in base pressure as h/R is increased from its two-dimensional value ($h/R = 0$) to an axisymmetric backstep with zero downstream wall radius ($h/R = 1$). Correspondingly, for flows with sudden expansion (Fig. 2c), base pressure values are lowered further. As h/R tends to $-\infty$, the base pressure would asymptotically approach zero if the downstream flow conditions continued to support supersonic continuum flow. As the base pressure decreased for higher Mach numbers at all values of h/R, so did its sensitivity to this measure of axisymmetry.

For both positive and negative values of h/R for Mach numbers of 2.09 and 3.02-3.90, agreement between experiment and FEM-FCT predictions is good, yielding an average difference of 12% (although no acceptable data was found for negative h/R values for Mach numbers above 2). Other computational results that sought to simulate the complete flowfield employed structured grids and empirical turbulence models without monotonic schemes and typically varied significantly from experiment in base pressure predictions as discussed by Petrie and Walker.[20] Two-dimensional predictions by Correa and Warren[21] exhibit strong overprediction (see Fig. 14) and indicate significant oscillations (1 contour level of variation along the base wall for 13 overall pressure contours in the flow). However, Uenishi et al.[22] indicate very good vertical traverse agreement at seven step heights downstream but do not present any base pressure predictions for the turbulent backstep flow. Analytical predictions by Zumwalt[14] show reasonable agreement with the experimental results. More recent analytic descriptions exhibit improved agreement and include Zelenkov[27] and Mueller,[2] who employed an empirical compressible divergence factor.

Reattachment Lengths

Another important characteristic observed in these flows is the flow reattachment length x_r, which is the downstream distance where the flow reattaches (see Fig. 1). Measurements taken by Roshko and Thomke[5] were derived from oil surface flow visualizations to determine the reattachment distance, whereas the predictions of x_r were defined as the point where the axial component of velocity along the downstream wall

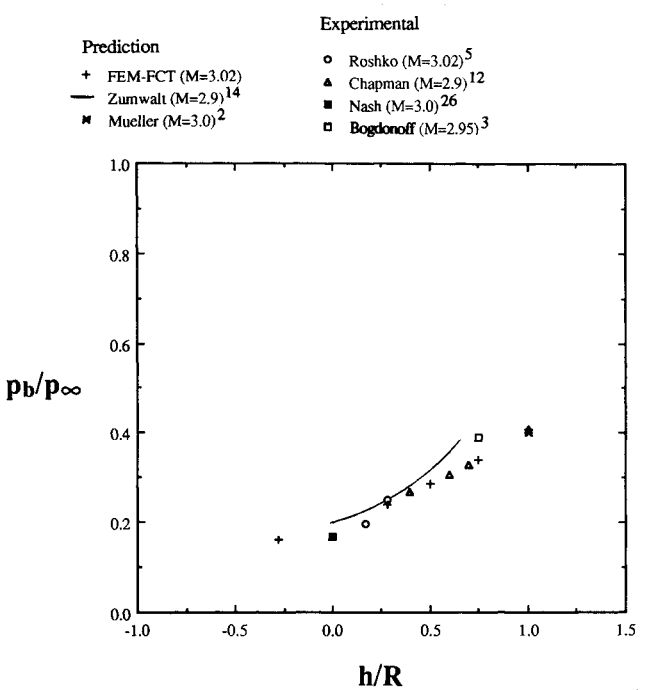

Fig. 15 Base pressure as a function of step height ratio (h/R) for $M_\infty = 3.02$

changed from negative to positive. Effects of axisymmetry were not clearly evident for x_r, since varying h/R for a given M_∞ produced roughly similar experimental and computational values for x_r. However, a general decrease in the average x_r was noted as M_∞ increased. The predicted average reattachment length distances normalized by h were 3.2, 2.8, and 2.1 for M_∞ of 2.09, 3.02, and 3.9, respectively (a similar trend was noted for median pressure distances, although the correlation was not as strong). The average difference between predicted and experimental values of x_r was 9%.[5] Such agreement indicates that reasonable prediction of the mixing layer inclination to the reattachment wall was found, demonstrating that the separated flow extent is largely controlled by the mixing layer recompression characteristics once the upstream corner separation is enforced.

The primary source of error in the calculations is expected to be the neglect of boundary-layer effects; however, some three-dimensional structures were also observed in the experiments[5] and may be important in capturing the full dynamics of the compressible mixing layer.[23,40] Future studies hope to examine the fluctuation properties and possible development and addition of a subgrid modeling for such an unstructured grid method.

Conclusions

Large eddy numerical simulations of an axisymmetric supersonic flow over a backward-facing step have been completed using an axisymmetric version of the finite element method-flux corrected transport algorithm. The adaptive unstructured remeshing provided detailed resolution in areas where rapid flow changes were occurring. Compressible flow features were found to be well represented by the conservative nonlinear FCT scheme when compared with available experimental results such as flow visualization, measurements of base pressure, and subsequent downstream wall pressure distribution as well as dimensionless reattachment lengths for a range of Mach numbers and step height to step radius ratios. Such reasonable agreement indicates that once separation at the corner is enforced, the general structure of the flowfield is determined largely by the presence of the transient mixing layer if flows with a thin turbulent upstream boundary layer are considered. Effects of increased axisymmetry (through increased step height to step radius ratio) were noted in flowfield characteristics such as increased base pressure ratios, curvature of expansion fans, stronger recompression shocks, and higher Mach number levels in the subsonic recirculating region. In general, such axisymmetric effects were less pronounced as the freestream Mach number was increased. In addition, the opposite trends were noted for sudden expansion flows.

Acknowledgments

The authors would like to acknowledge valuable discussions with J. Boris, R. Ramamurti, D. Fyfe, and G. Patnaik.

References

[1]Phillips, W. P., Findlay, J. T., and Compton, H. R., "Base Drag Determination for STS Flights 1-5," *Journal of Spacecraft and Rockets,* Vol. 23, No. 6, 1986, pp. 545-546.

[2]Mueller, T. J., "Determination of the Turbulent Base Pressure in Supersonic Axisymmetric Flow," *Journal of Spacecraft and Rockets,* Vol. 5, No. 1, 1968, pp. 101-107.

[3]Bogdonoff, S. M., "A Preliminary Study of Reynolds Number Effects on Base Pressure at $M = 2.95$," *Journal of the Aeronautical Sciences,* Vol. 19, March 1952, pp. 201-206.

[4]Donaldson, I. S., "The Effect of Sting Supports on the Base Pressure of a Blunt-Based Body in a Supersonic Stream," *Aeronautical Quarterly,* Vol. 6, Pt. 3, Aug. 1955, pp. 221-229.

[5]Roshko, A., and Thomke, G. J., "Observations of Turbulent Reattachment Behind an Axisymmetric Downstream-Facing Step in Supersonic Flow," *AIAA Journal,* Vol. 4, No. 6, 1966, pp. 975-980.

[6]Scherberg, M. G., and Smith, H. E., "An Experimental Study of Supersonic Flow over a Rearward Facing Step," *AIAA Journal,* Vol. 5, No. 1, 1967, pp. 51-56.

[7]Roshko, A., and Thomke, G. J., "Effect of Shoulder Modification on Turbulent Supersonic Base Flow," *AIAA Journal,* Vol. 5, No. 4, 1967, pp. 827-829.

[8]Donaldson, I. S., "On the Separation of a Supersonic Flow at a Sharp Corner," *AIAA Journal,* Vol. 5, No. 6, 1967, pp. 1086-1089.

[9]Hama, F. R., "Experimental Studies on the Lip Shock," *AIAA Journal,* Vol. 5, No. 2, 1968, pp. 212-219.

[10]Mishra, J. N., and Chatterjee, A. K., "Following Body Effects on Base Pressure in Supersonic Stream," *AIAA Journal,* Vol. 13, No. 6, 1975, pp. 732-735.

[11]Abu-Hijleh, B., and Saimimy, M., "An Experimental Study of a Reattaching Supersonic Shear Layer," AIAA Paper 89-1801, June 1989.

[12]Chapman, D. R., "An Analysis of Base Pressure at Supersonic Velocities and Comparison with Experiment," NACA TN 1051, Nov. 1956.

[13]Korst, H. H., "A Theory for Base Pressure in Transonic and Supersonic Flow," *Journal of Applied Mechanics,* Vol. 23, No. 4, 1956, pp. 593-600.

[14]Zumwalt, G. W., "Analytical and Experimental Study of the Axially-Symmetric Supersonic Base Pressure Problem," Ph.D. Dissertation, Dept. of Mechanical Engineering, Univ. of Illinois at Urbana-Champaign, Urbana, IL, 1959.

[15]Weiss, R., and Weinbaum, S., "Hypersonic Boundary-Layer Separation and the Base Flow Problem," *AIAA Journal,* Vol. 4, No. 8, 1966, pp. 1321-1330.

[16]Smith, J. H., and Lamb, J. P., "Eclectic Merger of Crocco-Lees and Chapman-Korst Approach to Near Wake," *International Journal of Heat and Mass Transfer,* Vol. 17, No. 12, 1974, pp. 1571-1589.

[17]Magi, E. C., and Gai, S. L., "Supersonic Base Pressure and Lipshock," *AIAA Journal,* Vol. 26, No. 3, 1988, pp. 370-372.

[18]Addy, A. L., Dutton, J. C., and Amatucci, V.A., "Nonuniform Nozzle Flow Effects on Base Pressure at Supersonic Flight Speeds, *AIAA Journal,* Vol. 24, No. 7, 1986, pp. 1209-1212.

[19]Shapiro, A. S., *The Dynamics and Thermodynamics of Compressible Fluid Flow,* Vol. II, Kreiger, Malabar, FL, 1983, p. 699.

[20]Petrie, H. L., and Walker, B. J., "Comparison of Experiment and Computation for a Missile Base Region Flowfield with a Centered Propulsive Jet," AIAA Paper 85-1618, July 1985.

[21]Correa, S. M., and Warren, R. E., "Supersonic Sudden-Expansion Flow with Fluid Injection: An Experimental and Computational Study," AIAA Paper 89-0389, Jan. 1989.

[22]Uenishi, K., Rogers, R. C., and Northam, G. B., "Numerical Predictions of a Rearward-Facing-Step Flow in a Supersonic Combustor," *Journal of Propulsion and Power,* Vol. 5, No. 2, 1989, pp. 158-164.

[23]Papamoschou, D., "Structure of the Compressible Turbulent Shear Layer," AIAA Paper 89-0126, Jan. 1989.

[24]Chien, K.-Y., Fergusen, R. E., Kuhl, A. L., Glaz, H. M., and Colella, P., "Inviscid Dynamics of Two-Dimensional Shear Layers," AIAA Paper 91-1678, June 1991.

[25]Löhner, R., Baum, J. D., Loth, E., Ramamurti, R., "A Finite Element Solver for Axisymmetric Compressible Flows," AIAA Paper 89-1794, June 1989.

[26]Nash, J. F., "A Review of Two-Dimensional Turbulent Base Flows," British Aeronautical Research Council, R&M No. 3323, March 1962.

[27]Zelenkov, O. S., "Flow in the Base Region in a Channel," *Fluid Mechanics—Soviet Research,* Vol. 10, March 1981, pp. 1-7.

[28]Blagosklonov, V. I., and Khomutov, V. A., "Sudden Expansion of a Supersonic Jet in a Cylindrical Channel," *Fluid Mechanics—Soviet Research,* Vol. 8, Jan. 1979, pp. 23-29.

[29]Löhner, R., Morgan, K., Peraire, J., and Vahdati, M., "Finite Element Flux Corrected Transport (FEM-FCT) for the Euler and Navier-Stokes Equations," *International Journal for Numerical Methods in Fluids,* Vol. 7, No. 10, 1987, pp. 1093-1109.

[30]Löhner, R., Morgan, K., and Peraire, J., "A Simple Extension to Multidimensional Problems of the Artificial Viscosity Due to Lapidus," *Communications in Applied Numerical Methods,* Vol. 1, No. 4, 1985, pp. 141-147.

[31]Löhner, R., "An Adaptive Finite Element Solver for Transient Problems with Moving Bodies," *Computers in Structures,* Vol. 30, No. 1/2, 1988, pp. 303-331.

[32]Löhner, R., Morgan, K., and Zienkiewicz, O. C., "An Adaptive Finite Element Procedure for High Speed Flows," *Computer Methods in Applied Mechanics and Engineering,* Vol. 51, No. 1-3, 1985, pp. 441-465.

[33]Baum, J. D., Loth, E., and Löhner, R., "Numerical Simulation of Shock-Elevated Box Interaction Using an Adaptive Finite-Element

Shock Capturing Scheme," *Proceedings of the 17th International Symposium on Shock Wave and Shock Tubes*, American Institute of Physics, New York, July 1989, pp. 909–914.

[34]Roe, P. L., "Error Estimates for Cell-Vertex Solvers of the Compressible Euler Equation," Institute for Computer Applications in Science and Engineering, ICASE Rept. 87-6, Hampton, VA, 1987.

[35]Oran, E. S., and Boris, J. P., *Numerical Simulation of Reactive Flow*, Elsevier, New York, 1987.

[36]Löhner, R., Morgan, K., Vahdati, M., Boris, J. P., and Book, D. L., "FEM-FCT: Combining Unstructured Grids with High Resolution," *Communications in Applied Numerical Methods*, Vol. 4, No. 6, 1988, pp. 717–730.

[37]Löhner, R., Morgan, K., and Zienkiewicz, O. C., *Accuracy Estimates and Adaptive Refinements in Finite Element Computations*, edited by I. Babuska, Wiley, New York, 1986, Chap. 15.

[38]Berger, M. J., and Oliger, J., "Adaptive Mesh Refinement for Hyperbolic Partial Differential Equations," *Journal of Computational Physics*, Vol. 53, No. 3, 1984, pp. 484–512.

[39]Mavriplis, D. J., "Accurate Multigrid Solution of the Euler Equations on Unstructured and Adaptive Meshes," AIAA Paper 88-3707, July 1988.

[40]Roshko, A., private communication, California Inst. of Technology, Pasadena, CA, 1989.

Gerald T. Chrusciel
Associate Editor